Universidad Zaragoza

End-of-degree project

Gold nanoparticles for radiotherapy and hadrontherapy

Author: Julia Espín Muñoz

Director: Piergiorgio Cerello

Director: Fernando Bartolomé Usieto

Academic course 2016/2017

September 2017

Contents

Chapter 1

Introduction

Cancer is a common pathology. Actually it is one of the major causes of death in the developed countries: statistics show that more than 14 million new cases are diagnosed in the world every year and that around 8.8 million people die of cancer [1]. There are several different and non-exclusive treatments, radiotherapy is one of the most common: it uses ionizing radiation to kill the cancerous tissue, leaving healthy tissue as less harmed as possible.
Medical physics appeared at the end of the 19th century with the discovery of the X-rays by Röntgen in 1895, the radioactivity by Becquerel in 1896 and the isolation of the Polonium and Radium by Pierre and Marie Curie in 1899. Within a few years, ionizing radiation started to be used with therapeutic aims [2].
Nowadays radiotherapy treatments in hospitals are delivered with a LINear ACcelerator (LINAC). It is used particle beams and photons at different energies. Less used is hadrontherapy, because of the high cost of the technology involved. Its beginnings date back to 1946 when Robert Wilson proposed the use of protons for cancer therapy. In contrast to radiotherapy that uses X-rays, hadrontherapy uses beams of heavy particles, called hadrons. The hadrons are typically protons and other ions, such as carbon. Thanks to their physical properties, hadrontherapy offers advantages when compared to radiotherapy, not only for the higher precision but also because of the greater biologic efficacy to kill certain tumorous cells [3].

1.1 Interaction between ionizing radiation and matter

Radiotherapy and hadrontherapy are based on the interaction processes between ionizing radiation and matter. Radiation is classified in ionizing radiation and non-ionizing radiation. When radiation passes through a material it interacts and loses energy. If the energy that is transferred to the matter is enough to produce ionization we talk of ionizing radia-

tion. It is classified in directly ionizing and indirectly ionizing. The first one involves charged particles (alpha and beta particles, protons, fission fragment ions) which ionize directly the particles of the medium, while in the second case the ionization happens through secondary charged particles produced by the passage of the primary radiation. In this category we find photons (X-rays and gamma rays) and neutral particles.

Interaction processes with matter differ depending on the radiation involved. The most commonly used ones in the biomedical field are electromagnetic radiation and charged particles. The interactions of X-photons and γ-photons with matter takes place through the photoelectric effect, the Compton effect, pair production, Rayleigh scattering and photonuclear interactions. A charged particle, when surrounded by its Coulomb electric force, interacts with one or more electrons or with the nucleus of every atom nearby. Heavy positively-charged particles interact primarily with matter through Coulomb forces between their charge and the negative charge of the orbital electrons of the absorber atoms.[4]
Whereas neutral radiation can pass through matter with little or no interaction, barely losing energy, charged particles interact through multiple collisions, losing only a small fraction of their kinetic energy in each one, gradually and continuously along the trajectory: at a certain distance, the loss of energy will be total. The range represents a distance beyond which no particle will penetrate. Therefore charged particles are characterized by a definite range in a given absorber material.
The linear stopping power, S, for charged particles in a given absorber is the differential energy loss per unit path length, for that particle within the material. Bethe and Bloch proposed a model for the collision stopping power using the Born approximation for the quantum mechanical calculation (1931). The Bethe-Block equation that describes the average energy loss for heavy charged particles is [5]:

$$S = -\frac{dE}{dx} = 4\pi N_A r_e^2 m_e c^2 \rho \frac{Z}{A}\frac{z^2}{\beta^2}[\frac{1}{2}ln(\frac{2m_e c^2\beta^2\gamma^2 T_{max}}{I^2}) - \beta^2 - \frac{\delta}{2}] \tag{1.1}$$

N_A: Avogadro number
ρ: Material density
r_e: Classical electron radius
β: $\frac{v}{c}$ of the particle
m_e: electron mass
γ: Lorentz factor of particles
I: Average ionization potential
Z: Atomic number
T_{maz}: Maximum energy transferable
z: Charge of primary particle
A: Atomic mass of the material
δ: Correction of high energy density

Several simplifications must be made at low energies while at high energies radiative effects are important. These limits of validity depend on both the effective atomic number of the absorber and the mass of the slowing particle. A minor dependence on the incident particle mass M at the highest energies is associated to T_{max}, but for all practical purposes in

high-energy physics dE/dx in a given material is only a function of β.

Just before a heavy charged particle loses all its kinetic energy, its energy loss per unit distance increases drastically and this results in a high dose deposition at that depth in the absorber. This high dose region appears close to the particle's range in the absorber and is named the Bragg peak. The depth depends on the type of particle and the energy. Thanks to this sharp dose deposition it is possible to target a well defined cancerous region at a certain depth by adjusting the energy of the incident particle beams. Consequently the damage to the healthy tissue will be minimized. In figure 1.1 is shown a schematic dose distribution for protons (135 MeV), photons (18 MV) and carbon ions (254 MeV/u and 300 MeV/u).

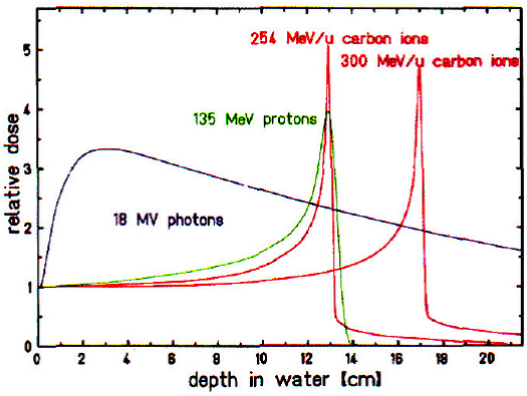

Figure 1.1: Dose profile of a charged particle beam compared to X-ray photons [6]

1.2 Radiobiology

Living organisms are continuously exposed to ionizing radiations from the natural background. In addition, there are exposures due to human activities, including the medical practices. Radiations are categorized into natural and man-made sources, but less than 10% of radiation exposure occurs on average from sources that are not natural [7]. With the development of the technology and the use of ionizing radiation, dosimetry and radiobiology were developed. The principal magnitudes of dosimetry are described in appendix A.

1.2.1 Ionizing radiation damage

The basis of radiotherapy and hadrontherapy are related to the damage produced to biological tissue when it is exposed to a ionizing radiation. The main target to which radiation induces severe damage and cell killing is the DNA molecule[11]. The DNA can be damaged:

- **Directly** through ionizations produced by the charged particles which cause base damage, single-strand breaks and double-strand breaks.
- **Indirectly** by the reaction of free radicals produced from water molecules.
  A free radical is an atom or molecule that carries an unpaired electron in the outer shell. As cells are composed of about 80% of water, the interaction with radiation is highly important. A water molecule may be ionized[7]

$$H_2O \rightarrow H_2O^+ + e^- \tag{1.2}$$

  H_2O^+ is an ion and a free radical. Its unpaired electron gives it a high chemical reactivity. The ion radical reacts with another water molecule to form $OH^\bullet$, which is even more reactive and can diffuse to reach a critical target cell.

$$H_2O^+ + H_2O \rightarrow H_3O^+ + OH^\bullet \tag{1.3}$$

  In the interaction process between water ionizing molecules, Reactive Oxygen Species (ROS) are produced. The quantity of ROS produced by the ionization of water depends on the PH and the radiation's LET. The hydroxyl radical ($OH^\bullet$) has a very short in vivo half-life ($\sim 10^{-9}s$) and high reactivity, which makes it a very dangerous compound to the organism. Moreover, it is estimated that about two thirds of the X-ray damage to DNA in mammalian cells is caused by it [12][13].

1.3 Nanotechnology and nanomaterials in biomedicine

Nanotechnology is a discipline in continuous development that deals with the creation, manipulation and application of structures characterized by at least one dimension in the nanometer range, commonly named nanomaterials. They are molecular or atomic agglomeration of 1-100 nm size.
There are promising applications of nanotechnology, one is nanomedicine, which creates nanoscale devices for improving therapy and diagnosis. Very influential is the use of nanoparticles, not only because of their size but also for the chemical composition, charge, structure and magnetic properties. Some of the applications of nanomaterials to biology and medicine are their use as fluorescent biological labels, drug and gene delivery, biodetection of pathogens and MRI contrast enhancement[14].

Nanoparticles are studied in different medical fields and can be engineered to have certain properties such as selectivity, size, shape and biocompatibility. Some of the possible medical applications of nanoparticles are the treatment of neurodegenerative diseases, HIV/AIDS, respiratory disases and cancer. One of the treatments for cancer is the use of nanoparticles

to increase the effect of radiotherapy [15]. In fact, this increase is the aim of this research work.

1.4 The nATT project

The nATT project (nanoAmplified Targed Therapy) investigates the use of nanoparticles to increase the radiotherapy effect. It is known that radiotherapy for cancer treatment has some limitations, such as the low efficiency against localized tumours, metastasised cancer or long-time problems. These limitations can be reduced by improving the effect of the radiation in the tumour target, reducing the effects in normal tissue. The nATT project aim is to use Gold NanoParticles (GNPs) as radiosensitizing agents for a future application in cancer radiation therapy. The collaboration groups are: the Istituto Nazionale di Fisica Nucleare (INFN), the Turin and Pisa University, the Turin Mauriziano hospital,the clinical physiological institute of the CNR of Pisa and the National Center of Oncological Hadrontherapy in Pavia (CNAO).
The objectives of this research are:

- The production, functionalization and characterization of GNPs.
- The study of the physics behind the radiosensitization induced by GNPs.
- The development of Monte Carlo simulation models to describe the GNP-induced radiosensitization.
- The uptake of functionalized GNPs and their kinetics in mice tumour, through micro-PET/CT imaging.

The nATT project started based on the results of several researches done by Kim and Hainfield [16][17], that showed how the presence of gold nanoparticles in tumour cells in mice increased the biological effect of the ionizing radiation (particularly for photon and proton beams) as shown in figure 1.2. The cited research works showed that the tumour control probability was greatly improved when irradiated metallic nanoparticles were present, in particular with gold nanoparticles.

1.4.1 Why the use of gold nanoparticles?

Because their properties make them suitable for the biomedical field:

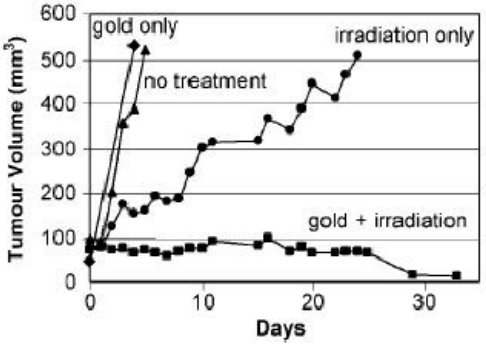

Figure 1.2: Average tumour volume after treatment with GNP and irradiation with photon beams.[16]

- Several studies show that GNPs can cause ROS production, cytotoxicity and apoptosis, also showing good biocompatibility.
- The process of synthesis and functionalization of GNPs of different sizes is quite simple and once prepared they are stable in time.
- Because of the high atomic number (Z_{Au}), GNPs can increase the absorption coefficient of the tissues in which they are present, making them usable as a imaging contrast agent [18].

1.4.2 Synthesis, characterization and functionalization of GNPs

The production and characterization of GNPs was performed at the Department of Molecular Biotechnology and Health Sciences of the University of Turin. There are different methods of GNP synthesis, they consist basically of two phases. Generally GNPs are produced in a liquid solution by reduction of chloroauric acid (H[AuCl4]), After dissolving (H[AuCl4]), the solution is rapidly mixed and a reducing agent is added. This causes Au^{3+} ions to be reduced to Au^{+} ions. To prevent the aggregation of particles, a stabilizing agent (citrate) that sticks to the nanoparticle surface is added. Citrate acts as a reducing agent as well as a capping agent to stabilize the GNPs through electrostatic interactions between the lone pair of oxygen electrons on the metal surface.
The method of synthesis used in the nATT project is the *Turkevich method*. It is based on the reduction of tetrachloroauric acid ($HAuCl_4$), produced by the oxidation of gold through hydrochloric acid combined with nitric acid or hydrogen peroxide, with sodium citrate, in water at 90º-100º C[19]. With this method 20nm size GNPs are produced. If the solution is stirred for a few minutes 5-10nm size GNP are produced.
The colloidal solution that is obtained is characterized by a ruby red colour: the intensity of colouring of the solution is directly related to the size of the obtained GNPs.

The size characterization is performed using a UV-visible spectroscopy, which measures the spectrum of absorbance. It can correlate the wave length of the absorption peak of the colloidal solution that contains GNPs (λ_{max}) with the average diameter of the nanoparticles inside it (d_{medio}). Transmission Electron Microscopy (TEM) and Scanning Electron Microscopy (SEM)are also used.

GNPs have been proposed as radiosensitizing agents in radiotherapy in future protocols. For this purpose the GNPs should concentrate inside the tumour agent selectively at the single cell level. So that the radiosensitizing action of the GNP is limited to the cancerous tissue, avoiding the amplification of the harm in the surrounding tissue. To achieve such selective concentration, the GNPs used to be functionalized with selective bio-markers. The bio-markers used in the nATT project are fluorodeoxyglucose (FDG) and Arginine-Glycine-Aspartic acid (RGD). The particularity in the functionalization used in the nATT project is the use of unspecific bio-markers. The attempt is that of use molecules that allow the accumulation of GNPs within as generic as possible a tumour target and not only in one part or typology, which is probable to happen if it is used very specified functionalizations.

1.4.3 GNPs as radiosensitizers

The basic idea for using GNPs as radiosensitizers is based on their ability to increase the dose deposited in the tumour target due to differences in their mass attenuation coefficient when compared to soft tissues, as shown in figure 1.3[20].

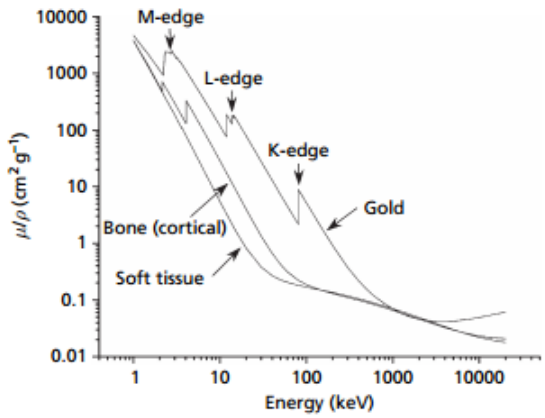

Figure 1.3: Plot of the mass attenuation coefficient for X-ray in soft tissue, bone and gold[16].

For photon energies in the order of KeV, the photoelectric effect is predominant and the

cross-section of this effect depends on the atomic number of the atom, scaling as Z^4. This means that the contribution of soft tissue to the total absorption is small while the ionization events in gold are expected to provide an important contribution [16]. Unfortunately, kilovoltage X-rays are also attenuated by soft tissue, with lengths on the order of 1cm. Consequently, the use of GNPs for a therapeutic advantage in combination with KeV radiation sources would be limited to relatively superficial tumours.

MeV X-rays interact with tissue primarily through the Compton effect, leading to a relatively homogeneous distribution of dose. However, the photoelectric effect is predominant for photon energies in the order of KeV. When Kev X-rays interact with gold, the photon is fully absorbed by an inner-shell electron, which then escapes from the gold atom[20]. After the ionizing event, low-energy secondary electrons are produced. These include a photo- or Compton electron with relatively high energy, followed by a shower of Auger electrons with much lower energies[21].

Auger electrons are characterized by energies relatively low: the major part presents an energy lower than 1 KeV while the total of the Auger electrons produced have energies lower than 10 KeV. The energetic spectrum of the Auger electrons does not substantially depend on the energy of the incident particle that leads the ionizing event, but on the energy of the atomic shell of which the photoelectron is emitted.

Several models (made by Sang Hyun Cho James L Robar Silvia A Riccio, MA Martin and some others) where used to calculate the increase of the dose deposit, on the basis of the gold concentration and of the processes of interaction with the incident radiation. Figure 1.5 shows that the correlation between the predicted dose and the observed radiosensitization is very weak with a correlation coefficient of $R^2 = 0.08$ [20]. In bulk gold, the majority of the low-energy electrons are stopped immediately within the gold. In contrast, for GNPs a large portion of these low-energy electrons have sufficient energy to scape and deposit their energy very densely in the vicinity of the nanoparticle, leading to high doses and many ionizing events in a small volume[21].

In the vicinity of a nanoparticle, Auger electrons produce the dominant contribution to dose, but this decreases rapidly with the distance. The reduced energy of Auger electrons results in a restricted range of interaction and responsible of the major contribution to the dose deposit near the nanoparticles.

This size effect diminishes at longer ranges, as dose deposited far from the nanoparticle is the result of photo-electrons and energetic Auger electrons, which easily escape from nanoparticles of any size[21]. It can be seen in figure 1.4.

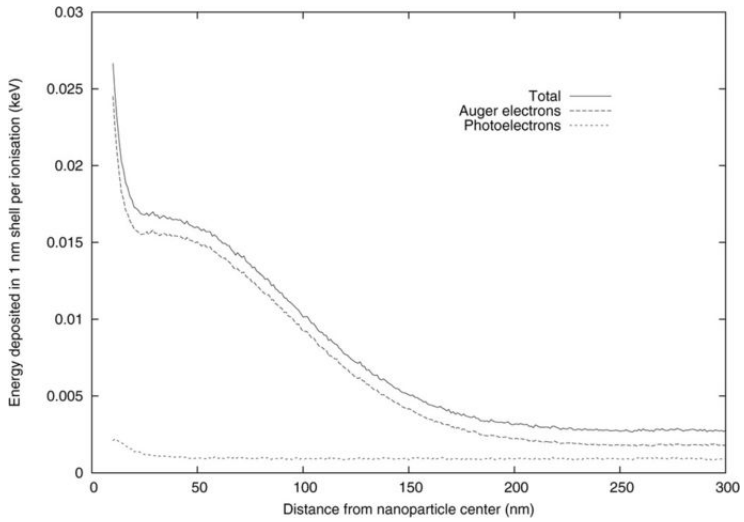

Figure 1.4: Average energy deposit in the vicinity of a 20nm GNP after a singe ionising event by a 40 KeV photon[21].

The disparity between the experimentally observed radiosensitization and dose enhancement based on physical predictions shown in figure 1.5 suggests a strong biological component to the mechanism of radiosensitization.

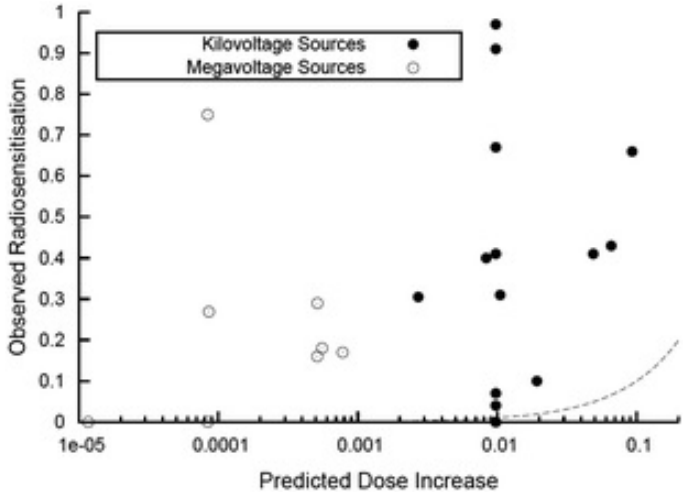

Figure 1.5: Correlation between the predicted doseincrease and observed experimentally in presence of GNPs[20].

The main biochemical mechanism of radiation induced cell death is the action of free radicals. The hydroxyl radical ($OH^{\bullet}$) is the main responsible of indirect DNA damage. Metallic nanoparticles are known to induce the production of ROS leading to oxidative stress. In combination with ionizing radiation some experimental reports have observed an elevated oxidative stress. Some experiments suggest that ROS production may be a good candidate to explain the biological component of radiosensitization that is induced by GNPs [20].

1.4.4 Results of previous researches

Previous research in the nATT project has studied the production of ROS induced by radiotherapy irradiation with photon beams of samples containing GNPs at different concentrations and at different sizes. The study was carried out in physiological condition, so the samples subject to irradiation were prepared in PBS with a physiological PH. The irradiated samples, were synthesized with the *Turkevich method*, functionalized with citrate and had three different molar concentrations ($0\mu M$, $5\mu M$, $10\mu M$) and three different sizes (5nm, 10nm, 20nm). Also, in order to determinate quantitatively the hydroxyl radical in the solution, it was measured the terephthalate (TPA) fluorescence. Previous tests used also 1,3Diphenylisobenzofuran (DPBF), but TPA was the most reliable probe.

Results for 20nm size showed that there was no production increase of hydroxyl radicals with the increasing of the GNPs evidence of concentration in the analysed samples, so the next measurements were developed only for 5nm size. In this case it was seen that the fluorescence signal in samples containing GNPs increased, so there was an increase of the hydroxyl radical production. The comparison between two intensity ratios (R5 and R10, that are the fluorescence intensity at a specific dose of the sample with concentration $5\mu M$ over $0\mu M$ and $10\mu M$ over μM respectively, this ratios are fully explained in chapter 3) showed an excess production of hydroxyl radicals, which did not happen with the 20nm size GNPs. This is in agreement with the hypothesis for which there is a proportionality in production of radicals with the ratio surface or volume of the nanoparticle: smaller nanoparticles allow Auger electrons to escape from the bulk of the nanoparticle, in comparison with larger nanoparticles. The measurements taken with the 10nm size nanoparticles were similar to those with the 20 nm.
The larger is the size of the nanoparticle, the smaller the probability that an ionizing event will generate Auger electrons able to escape from them. On the contrary, for smaller nanoparticles the Auger electrons will be able to escape from the nanoparticle and generate ionization that increases ROS production.

1.5 Next objectives

After the obtained results, now, what we have done is carrying out measurements with hadron beams for gold nanoparticles, in order to compare the results obtained with photon beams and try to gain a beter understanding of the GNP sensitization mechanism. To do it proton and carbon ions are used.

Chapter 2

Irradiation procedure and instrumentation

This research work, developed in the framework of the nATT project explores the GNP-induced ROS production, with respect to the standard treatment conditions in hadrontherapy.
It is studied whether or not the increase of free oxygen radicals could represent a chemical-biological component in the radiosensitization induced by the GNPs. The measurement of ROS production is the first problem to solve due to their very short lifetime ($\sim 10^{-9} s$) and the variety of antioxidants existing in vivo that can capture them. Therefore a protocol was developed to quantify the reactive oxygen species.
There are several methods to measure the ROS. Fluorescent probes was the one used in this project.

2.1 The fluorescence phenomenon

Fluorescence and phosphorescence are photon emission processes that occur during atomic and molecular relaxation from electronic excited states. These photonic processes involve transitions between electronic and vibrational states of polyatomic fluorescent molecules called fluorophores [22]. They can absorb electromagnetic energy with a specific wavelength and re-emit electromagnetic radiation to a different wavelength from that absorbed [23]. The electronic excited states of a polyatomic molecule can be further classified based on their multiplicity.

The phenomenon of fluorescence displays a number of general characteristics:

- **The Stokes Shift.** It describes the observation that fluorescence photons are longer in

wavelength than the excitation radiation.

- **Kasha's rule.** Same fluorescence emission spectrum is generally observed irrespective of the excitation wavelengths.
- **Temperature effect.** On increasing the temperature, higher vibrational levels of the ground state are populated according to the Boltzmann distribution and more transitions occur from lower to higher vibrational levels of the first excited electronic state. As a result the absorption spectrum becomes broader and the superposition of the different levels blurs most of the vibrational fine structure of the band.[24]
- **Quenching.** The intensity of fluorescence can be decreased by a wide variety of processes. The two main types are collisional quenching, that occurs when the excited-state fluorophore is deactivated upon contact with some other molecule in the solution, the quencher, and static quenching in which fluorophores can form nonfluorescent complexes with quenchers[25].

2.2 Spectroscopic techniques

2.2.1 Ultraviolet-visible spectroscopy

The (UV-visible) spectrofluorometry is a spectroscopic technique used for the study of ROS production in samples with GNPs.
This technique is used for characterizing the GNP sizes after preparation.
Fluorometry has been used for the measure of the fluorescence signal during interaction between hydroxyl and TPA.

Ultraviolet-visible spectroscopy is used to obtain the absorbance spectra of a compound in solution or as a solid[24]. Because light is a form of energy, the light absoption of the matter causes the increase of the atomic or molecular energy. The total potential energy of a molecule generally is represented as the sum of its electronic, vibrational and rotational energies:

$$E_{molecule} = E_{electronic} + E_{vibrational} + E_{rotational} \tag{2.1}$$

Where:

$$E_{electronic} > E_{vibrational} > E_{rotational} \tag{2.2}$$

In molecules and atoms, photons of UV and visible light have enough energy to cause transitions between the different electronic energy levels [26].
In an ultraviolet-visible spectroscopy, a light beam hits in the sample, part of this light will

be absorbed while the rest will be transmitted.
The Beer-Lambert law states that the absorbance of a solution is directly proportional to the concentration of the absorbing species in the solution and to the path length. Thus, for a fixed path length, UV/Visible spectroscopy can be used to determine the concentration of the absorber in a solution. The Beer-Lambert law expresses a linear relationship between absorbance and concentration[27]. It describes the absorption of solutions of small concentrations ($< 10mM$). At higher concentrations, the analyte begins to behave differently due to interactions with the solvent and other molecules and sometimes even due to hydrogen bonding interactions.

2.2.2 Spectrofluorimetry and spectrofluorimeter

Spectrofluorimetry is a technique of quantitative chemical analysis. Fluorescent compounds have two characteristic spectra: an excitation and an emission spectrum. This technique has many advantages such as sensitivity, specificity, linearity and simplicity.

The spectrofluorimeter is the instrument used to measure fluorescence. It generates the wavelength of light required to excite the analyte of interest; it selectively transmits the wavelength of light emitted and measures its intensity. The emitted light is proportional to the concentration of the analyte being measured. The most common light source for fluorometers are lamp sources. They provide a relatively uniform intensity over a broad spectrum range from the ultraviolet to the near infrared. The optical paths of the excitation and the detection light paths are along orthogonal axis. The orthogonal arrangement ensures a minimal leakage of excitation light onto the detection side[22][25]. Emission slits and excitation slits are are used to adjust the intensity of the fluorescent light that impinge on the detector and the excitation incident in the sample respectively. The excitation filter selects a range of wavelengths from a broadband source to excitate the sample. The emission filter transmits the emission and rejects the excitation wavelengths. The most common detectors used for sample analysis are photomultipliers and photodiodes, with an amplifier system and digitalization signal.

2.3 Procedure main steps

1. Sample preparations with gold nanoparticles and a fluorescent probe.
2. Sample irradiation, carried out at CNAO in Pavia.
3. Sample analysis to evaluate ROS production following the irradiation.

The samples to be irradiated are prepared in 1.8 ml vials. Samples are composed by PBS (phosphate buffered saline), gold nanoparticles (GNPs) and probe (TPA, terephthalic acid). In the nATT project we want to reconstruct in vitro a condition as closer to human physiology as possible. So the study of ROS production in GNP samples must be carried out in physiological condition. The samples subject to irradiation are prepared in phosphate buffered saline (PBS) with a physiological PH between 7.35 and 7.45, the range of cellular citosol. The PBS used is called Gomori PBS, it is a water solution containing two salts(one acid and one basic): KH_2PO_4 (potassium dihydrogen phosphate and K_2HPO_4 (potassium phosphate dibasic. The concentrations of the slats are (0.56 ± 0.01)mM and (1.4 ± 0.03)mM respectively.
The irradiated samples are prepared with three different GNP molar concentrations: 0μM, (5±0.03)μM and (10±0.07)μM. In this case we use gold nanoparticles of (5 ± 2)nm and (20 ± 2)nm of diameter. The molar concentration or molarity (M) is a measure of the concentration of a solute in a solution:

$$Molarity = \frac{Solute\ Mols}{Solution\ Volume} \tag{2.3}$$

$$Solute\ Mols = \frac{Solute\ Mass}{Solute\ Molar\ Mass} \tag{2.4}$$

The samples are shown in figure 2.1:

Figure 2.1: Samples with the different concentrations. From left to right: 0μM, 5nm; 5μM, 5nm; 10μM, 5nm; 0μM, 20nm; 5μM, 20nm; 10μM, 20nm.

The gold nanoparticles have been specifically prepared with citrate to stabilize their size. The samples, containing GNPs and fluorescent probes in PBS, are prepared in plastic vials made of polypropylene, a material with density similar to water. This is a very important characteristic because during irradiations the samples are inserted in a body human simulator (so called a 'phantom'), so that the dose deposited is not perturbed by the vials.

TPA or Terephthalic acid is an aromatic compound, which has a strong fluorescence with

wavelengths

$$\lambda_{excitation} \approx 310nm \qquad \lambda_{emission} \approx 430nm \tag{2.5}$$

Terephthalic acid is not fluorescent, but it becomes fluorescent if it binds to the hydroxyl radical: during this interaction TPA turns in to 2-hydroxytere-phthalic acid (HTPA). The HTPA fluorescence is measured with a spectrofluorimeter, which allows the quantitative determination of hydroxyl radical in the analysed solution.

2.4 Irradiation

The experiment took place at CNAO (National Center of Oncological Hadrontherapy) in Pavia, by irradiating the samples with GNPs in the standard conditions used in hadrontherapy. The samples have been irradiated by a synchrotron producing both proton beams and carbon ion beams with the energies show in table2.1.

Figure 2.2: First: Treatment room Second: Synchrotron

Radiation type	Dose (Gy)
Proton	1,2,4
Carbon ions	1,2,3,4

Table 2.1: Radiation and energy used

The synchrotron used is a particle accelerator 80 meters long with a diameter of 25 meters. The particles are accelerated up to kinetic energies of 250 MeV for protons and 480 MeV for carbon ions.
The particle beam is accelerated in the synchrotron and travels about 30,000 kilometers in a half second to reach the desired energy. The beams are then sent to the treatment room.

In this case the target is situated at 14,6 cm of depth in water. The phantom has been irradiated in an area of 12x12cm^2 for carbon ions and 9x9cm^2 for protons. The configuration is shown in figure 2.3.

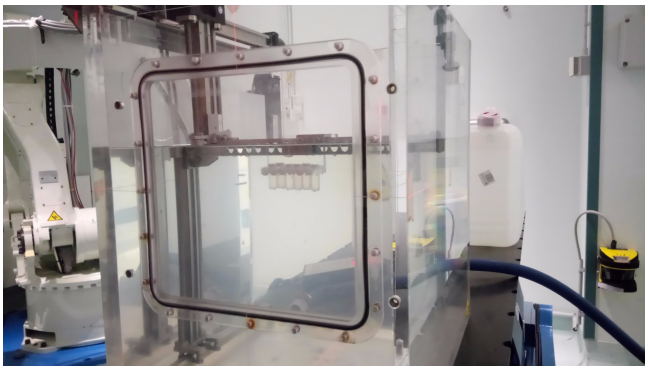

Figure 2.3: Setup

2.5 Samples analysis

One of the most important problems has been the fact that the spectrofluorimeter that we were supposed to use in Pavia did not work well. So we had to freeze the samples and then come back to Turin in order to analyse them. These has given several problems because the samples might not have been preserved optimally and although it has been tried to follow the same time intervals for all the samples during freezing and defrost, they have not been exactly the same. Despite that, the results suggest interesting trends discussed in the next chapter.

Chapter 3

Data analysis

In this chapter are presented the results of $OH^{\bullet}$ production, in samples containing GNPs of different sizes, and subject to irradiation with protons and carbon ion beams. In this research work TPA is the probe used to measure the $OH^{\bullet}$ production.
In literature there are no studies in which the TPA has been used to measure the production of $OH^{\bullet}$ in samples containing GNPs in standard condition of irradiation, so in the nATT project a protocol was developed. They studied the TPA stability and the optimal TPA concentration. On the one hand, for eight hours, the TPA trend can be considered stable enough. On the other hand, the TPA concentration must be sufficient to measure all $OH^{\bullet}$ radicals without saturation phenomena. The optimal TPA concentration was studied in samples without GNPs, subject to irradiation with different doses. As expected the fluorescence signal increases with the increasing probe concentration, and it is linear with the irradiation dose. The optimal TPA concentration was chosen as the one providing the largest sensitivity: $(1.00 \pm 0.01)\,mM$.

3.1 GNPs 5nm and 20nm size

Between the irradiation and the sample analysis, samples were not exposed to light, in order to minimize the possible signal deterioration. The results are shown below:

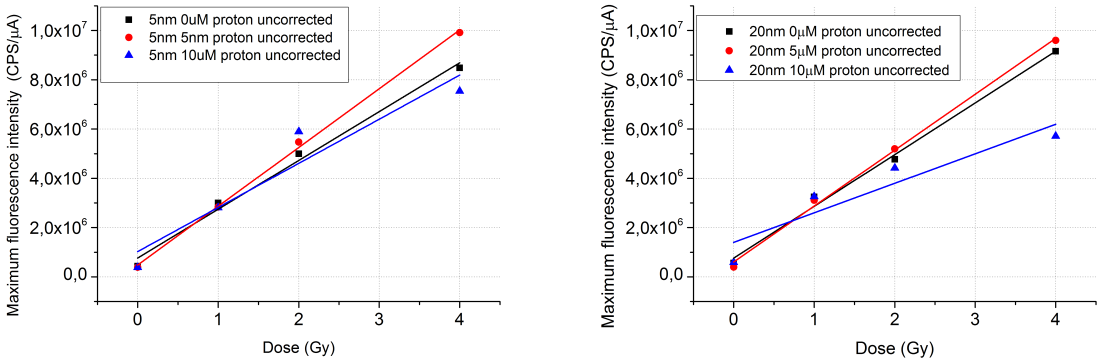

Figure 3.1: Measurements of the fluorescence intensity of the samples with 5nm and 20nm respectively and without correction for proton beams.

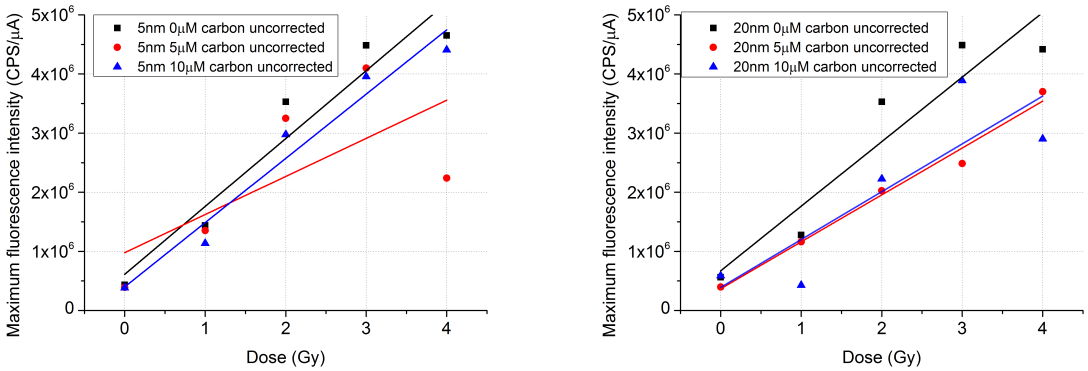

Figure 3.2: Measurements of the fluorescence intensity of the samples with 5nm and 20nm respectively and without correction for carbon ion beams.

Signal saturation is not observed, suggesting that the concentration of probe (TPA) in the sample is sufficient to react with all OH radicals produced as a result of irradiation.
Also, it is seen hat the intensity of fluorescence increases linearly with the dose, except for some samples that will be commented later.
An unexpected decrease of the HTPA fluorescence signal with the increase of the GNP concentration in samples is observed in figures 3.1 and 3.2.
Different hypothesis have been made to explain the causes of this phenomenon which cannot be associated to an actual decrease of the concentration of the OH radical.

3.2 Correction factor

Several effects were considered in a previous research in the nATT project which may lead to the behaviour observed in figures 3.1 and 3.2. For each effect a correction method was developed and applied to the data. Firstly, it was considered the absorption of the light signal emitted by the HTPA by GNPs, but the correction did not apported a correction to the data. Secondly, it was considered the adsorption between HTPA and citrate but it had a negligible effect.
The last effect considered was the light diffusion by GNPs and it had a great importance in the data correction. Its possible influence was studied by characterizing the EM slits. The sensitivity of the spectrofluorometer is determined by the emission slit (EM slit). The EM slit determines the intensity fluorescence signal that reaches the detector. The spectrophotometer used has a full scale of 1000 a.u. The dependence of the measured signal on the opening of EM slits is studied analysing non irradiated samples containing TPA and different concentration of GNPs. The spectrofluorometer settings are reported in the table 3.1.

Scan speed (nm/min)	100
$\lambda_{excitation}$ (nm)	304
EX Slit (nm)	5.0
EM Slit (nm)	(5,5.5,6.2,6.4,7,8.5,10)
Fluorescence spectrum	360-460

Table 3.1: Spectrofluorimeter settings

In order to compare for statistical fluctuations five sets of identical samples for every concentration of GNPs were measured. The analysis of samples was made by scanning as a function of an increasing EM slit opening.
The fluorescence signal as function of the opening EM slits showed a parabolic trend for all concentrations of GNPs. Thanks to these studies, a correction factor was determined. The average trend of maximum fluorescence intensity as a function of the opening EM slits has allowed to determine a correction factor to apply to measurements. Since for no irradiation the same fluorescence signal for all samples is expected independently of the concentrations of GNPs, the ratio of the signal with no GNPs and with GNPs concentration provides correction factors to be applied to raw data on irradiated samples.
An integrated corrective factor was calculated:

$$C_{5\mu M}(EM\ Slits) = \frac{I_{0\mu M}}{I_{5\mu M}} \qquad C_{10\mu M}(EM\ Slits) = \frac{I_{0\mu M}}{I_{10\mu M}} \tag{3.1}$$

$I_{0\mu M}$ is the fluorescence intensity measured with opening of the EM slits for the GNP concentration 0 μM, $I_{5\mu M}$ for 5 μM and $I_{10\mu M}$ for 10 μM.

For 20nm GNPs the correction factor is:

$$C_{5\mu M}(6.4nm) = 1.10 \pm 0.04 \qquad C_{10\mu M}(6.4nm) = 1.16 \pm 0.05 \tag{3.2}$$

For 5nm GNPs the correction factor is:

$$C_{5\mu M}(6.2nm) = 1.48 \pm 0.07 \qquad C_{10\mu M}(6.2nm) = 1.88 \pm 0.09 \tag{3.3}$$

The corrected measurement is obtained by multiplying the intensity of irradiated samples at $5\mu M$ and $10\mu M$ for the corresponding correction factor.

$$Correction\ for\ 5\mu M \qquad I_{max\,5\mu M} * C_{5\mu M} \tag{3.4}$$

$$Correction\ for\ 10\mu M \qquad I_{max\,10\mu M} * C_{10\mu M} \tag{3.5}$$

The application of the correction factor to the measurements is shown in figures 3.3 and 3.4 while in figures 3.5 and 3.6 is shown the comparison of maximum fluorescence intensity as a function of dose; between incorrect and correct values. It is important that this time the spectrofluorimeter was not the same used the last time that the correction factors were calculated so the correction factors, although similar, might not be exactly the same. In order to correct them better they should be recalculated.

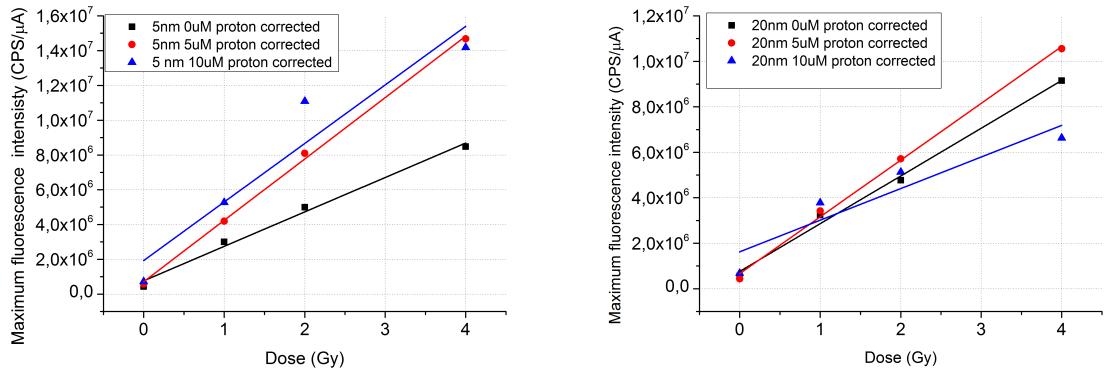

Figure 3.3: Measurements of the fluorescence intensity of the samples with 5nm and 20nm respectively and corrected for proton beams.

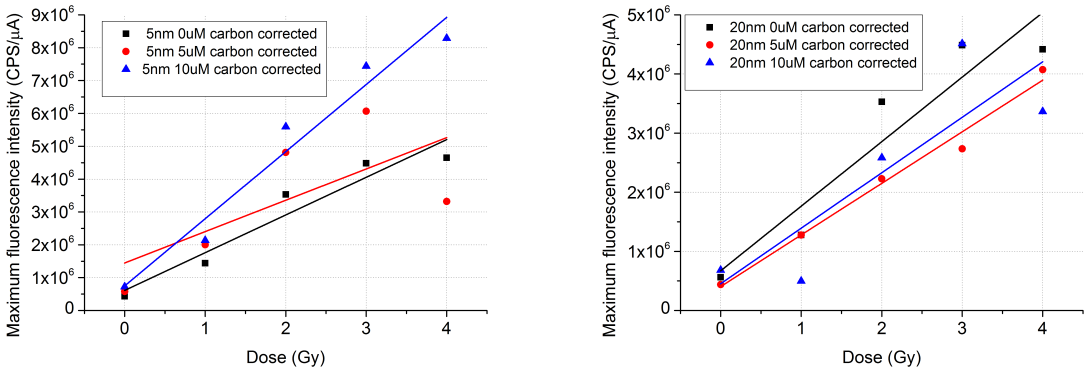

Figure 3.4: Measurements of the fluorescence intensity of the samples with 5nm and 20nm respectively and corrected for carbon ion beams.

Comparison between corrected and uncorrected data:

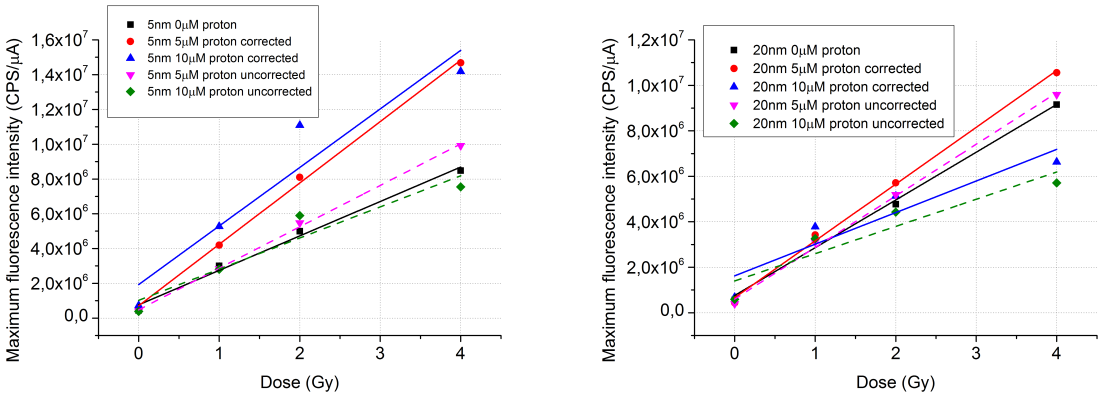

Figure 3.5: Measurements of the fluorescence intensity of the samples with 5nm and 20nm GNPs respectively and corrected for proton beams.

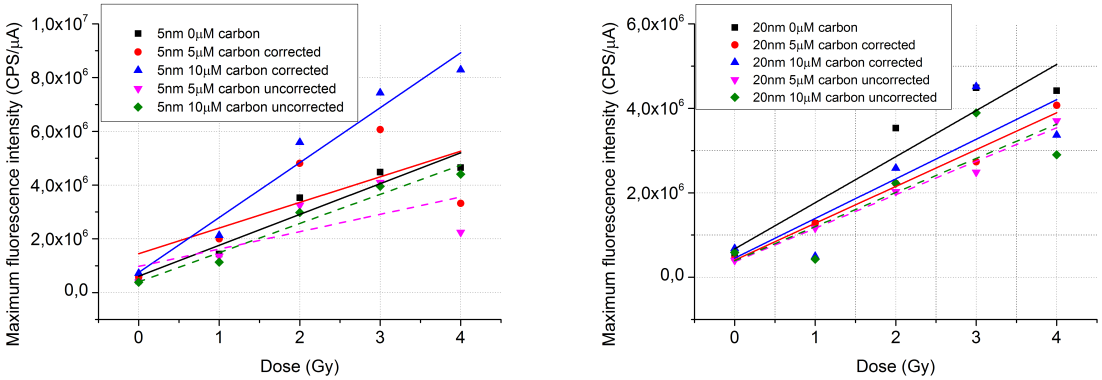

Figure 3.6: Measurements of the fluorescence intensity of the samples with 5nm and 20nm GNPs respectively and corrected for carbon ion beams.

The effect of the GNPs concentration of hydroxyl radical production is studied through the relationship between the fluorescence intensity of HTPA samples containing gold nanoparticles and samples in which there are no gold nanopaticles. In this way it can be understood the relative production of OH radicals in presence of GNPs, according to the concentration of nanoparticles and the irradiation dose. These relationships are defined by equations:

$$R_5(dose) = \frac{I_{max\,5\mu M}(dose)}{I_{max\,0\mu M}(dose)} \qquad R_{10}(dose) = \frac{I_{max\,10\mu M}(dose)}{I_{max\,0\mu M}(dose)} \tag{3.6}$$

where $I_{max\,i\mu M}(dose)$ is fluorescence intensity at a specific dose of the sample with GNP at concentration $i\ \mu M$.

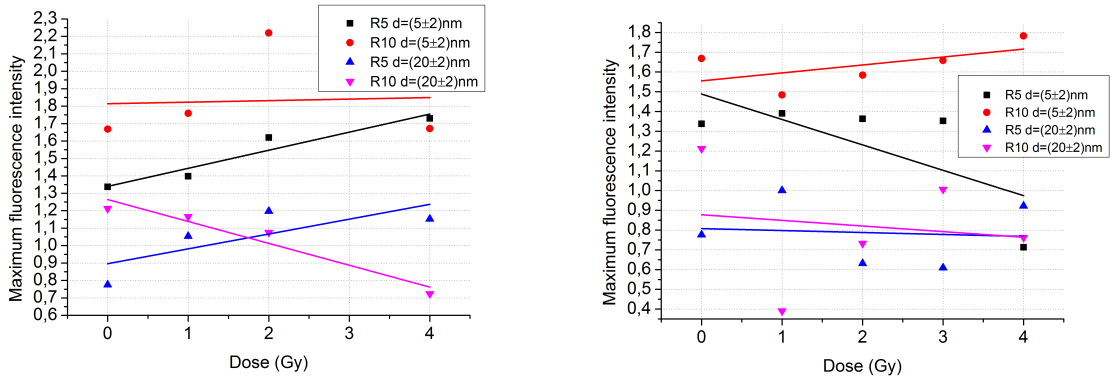

Figure 3.7: Ratio of fluorescence intensity of the samples of 5nm and 20nm as a function of the dose for proton and carbon ion beams respectively.

The experimental points are interpolated with a linear fit, as a function of the irradiated dose.

In the case of 20nm for carbon ions it can be concluded that there is no production of OH radicals with the increasing of the concentration of GNPs in the analysed samples. The lines of R5 for 20nm and 5nm for protons show an effective increasing as a function of the irradiated dose.

The comparision between two intensity ratios show an excess production of hydroxyl radicals in samples with nanoparticles at 5nm for protons. Probably for carbon are the same, it seem to be like it except for the sample irradiated at 4 Gy, that might have suffered some contamination.

This phenomenon is compatible with the hyphothesis for which there is a proportionality in production of radicals with the ratio surface to volume of the nanoparticle.

Conclusions

This research work was carried out within the nano Amplified Targeted Therapy(nATT) project. Its aim was to measure the production rate of Reactive Oxygen Species (ROS) in samples containing Gold Nano Particles (GNPs), of different sizes, and subjected to irradiation with photon, proton and carbon ion beams. Measurements were focused on the hydroxyl radical (•OH) because it is considered the most important source of indirect damage caused by the interaction between ionizing radiation and biological matter.
The concentration of hydroxyl radical, which is mainly responsible for damage to macromolecules such as DNA and proteins, was measured using a fluorescent probe: sodium terephthalate (TPA). All the measurements were made at the National Center of Oncological Hadrontherapy by irradiating samples with proton beams and carbon ion beams produced by a synchrotron.
The OH production after irradiation was studied in samples containing GNPs at $0\mu M$, $5\mu M$ and $10\mu M$ concentration. The study was done for two different sizes of GNPs diameter: 20 nm and 5 nm. The results obtained with the use of GNPs by the average diameter of 5 nm show an excess production of hydroxyl radicals for both proton and carbon ion beams. However for 20 nm, it is only seen for proton beams.
When comparing these results with the ones obtained for radiotherapy it is seen that GNPs might have a better use in hadrontherapy rather than in radiotherapy because they have a more pronounced effect in the last one, making its use in hadrontherapy more promising. This cannot be concluded yet, further research has to be done.
The future steps are carrying out more measures with hadron beams for gold nanoparticles, so as to compare the results obtained and hopefully gain further understanding on the GNP sensitization mechanism.
In September more experiments are going to be developed at CNAO.

Bibliography

[1] World Health Organization, 2017.

[2] Eric J. Hall and Amato J. Giaccia. *Radiobiology for the radiologist.* Lippincott Williams and Wilkins, 2006.

[3] E. Herranz, J. L. Herraiz, E. Vicente, S. España, J. Cal-González, J. M. Udías. *Hadronterapia*, 2008.

[4] Frank H. Attix. *Introduction to Radiological Physics and Radiation Dosimetry*, by John Wiley & sons, p 160, ISBN: 978-0-471-01146-0, 1986.

[5] Hans A. Bethe and Julius Ashkin. Passage of radiations through matter. *Experimental nuclear physics, 1 (part II)*:309, 1953.

[6] Weber U, Kraft G. *Comparison of carbon ions versus protons.* Cancer J. 15(4):325-32, 2009.

[7] Saman Khaled and Kathryn D. Held. *Radiation biology: a hand book for teachers and students.* International Journal of Radiation Biology, 88(11):858-859, 2012.

[8] Absorbed Dose ICRU. Report 85. International Commission on Radiation Units and Measurements. Fundamental Quantities and units for ionizing radiation (Revised), 2011.

[9] International Atomic Energy Agency. *Technical report series n.461: Relative biological effectiveness in ion beam therapy*, 2008.

[10] Linear Energy Transfer ICRU. Report 85. International Commission on Radiation Units and Measurements. Fundamental Quantities and units for ionizing radiation (Revised), 2011.

[11] M.E. Lomax, L.K. Folkes and P. O'Neill.*Biological consequences of radiation-induced DNA damage: Relevance to radiotherapy*, 25(10):578-85 2013.

[12] Aaron K. Holley, Lu Miao, Daret K. St. Clair and William H. St. Clair. *Rodox-modulated phenomena and radiation therapy: The central role of superoxide dismutases.*20(10): 1567-1589, 2014.

[13] Paul Held. *An introduction to reactive oxygen species. Measurement of ROS in cells.* Bioteck Application Guide, pages 1, Äì14 2012.

[14] Carolyn M. D'almeida and Bradley J. Roth. *Medical applications of nanoparticles*, Department of Physics, Oakland University, Rochester, Michigan, 2013.

[15] Shashi K. Murthy. *Nanoparticles in modern medicine: State of the art and future challenges.*International journal of nanomedicine, 2(2):129, 2007.

[16] James F. Hainfeld, F. Avraham Dilmanian, Daniel N. Slatkin and Henry M. Smilowitz. *Radiotherapy enhancement with gold nanoparticles.* Journal of Pharmacy and Pharmacology 60:977-985, 2008.

[17] Kim et al. *Enhanced proton treatment in mouse tumours through proton irradiated nanoradiator effects on metallic nanoparticles.* Phys. Med. Biol. 57:8309-8323, 2012.

[18] JF. Hainfeld, DN. Slatkin, TM. Focella, and HM. Smilowitz. *Gold nanoparticles: a new x-ray contrast agent.* The British journal of radiology, 2014.

[19] J. Kimling, M. Maier, B. Okenve, V. Kotaidis, H. Ballot, and A. Plech. *Turkevich method for gold nanoparticle synthesis revisited.* The Journal of Physical Chemistry B, 110(32):15700-15707, 2006.

[20] Karl T. Butterworth, Stephen J. McMahon, Fred J. Currell, and Kevin M. Prise. *Physical basis and biological mechanisms of gold nanoparticle radiosensitization.* Nanoscale, 4(16):48304838, 2012.

[21] Stephen J. McMahon, Wendy B. Hyland, Mark F. Muir, Jonathan A. Coulter, Suneil Jain, Karl T. Butterworth, Giuseppe Schettino, Glenn R. Dickson, Alan R. Hounsell, Joe M. O'Sullivan, et al. *Biological consequences of nanoscale energy deposition near irradiated heavy atom nanoparticles.* Scientific reports, 1, 2011.

[22] Peter TC So and Chen Y Dong. Fluorescence spectrophotometry. eLS, 2002.

[23] Markus Sauer, Johan Hofkens, and Joerg Enderlein. Basic principles of fuorescence spectroscopy. Handbook of Fluorescence Spectroscopy and Imaging: From Single Molecules to Ensembles, pages 1-30, 2011.

[24] Brittany L Oliva-Chatelain and Andrew R Barron. Basics of uv-visible spectroscopy.

[25] Joseph R Lakowicz. Principles of fuorescence spectroscopy. Springer Science and Business Media, 2013.

[26] A Primer. Fundamentals of uv-visible spectroscopy. Copyright Hewlett-Packard Company, Hewlett-Packard publication, (12- 5965).

[27] DF Swinehart. The beer-lambert law. Journal of chemical education, 39(7):333, 1962.